

Emergent Spatial Textures from Interaction Quenches in the Hubbard Model

Sankha Subhra Bakshi¹ and Gia-Wei Chern¹

¹*Department of Physics, University of Virginia, Charlottesville, Virginia, 22904, USA*

(Dated: January 30, 2026)

Interaction quenches in strongly correlated electron systems provide a powerful route to probe nonequilibrium many-body dynamics. For the Hubbard model, nonequilibrium dynamical mean-field theory has revealed coherent post-quench oscillations, dynamical crossovers, and long-lived transient regimes. However, these studies are largely restricted to spatially homogeneous dynamics and therefore neglect the role of spatial structure formation during ultrafast evolution. Here we investigate interaction quenches in the half-filled Hubbard model using a real-space time-dependent Gutzwiller framework. We show that homogeneous nonequilibrium dynamics is generically unstable: even arbitrarily weak spatial fluctuations grow dynamically and drive the system toward intrinsically inhomogeneous states. Depending on the interaction strength, the post-quench evolution exhibits spatial differentiation, nucleation, and slow coarsening of Mott-like domains. Our results establish spatial self-organization as a generic feature of far-from-equilibrium correlated matter and reveal a fundamental limitation of spatially homogeneous nonequilibrium theories.

The nonequilibrium dynamics of strongly correlated electron systems have attracted intense interest over the past decade, driven largely by rapid advances in ultrafast experimental techniques [1–4]. Modern pump–probe and time-resolved spectroscopies now access femtosecond time scales, enabling direct observation of electronic, magnetic, and lattice dynamics far from equilibrium [5–8]. Importantly, nonequilibrium perturbations are no longer employed merely as diagnostic probes [9], but have emerged as powerful control knobs to engineer and manipulate quantum states of matter.

While driven systems display rich phenomenology, a deeper theoretical understanding is facilitated by focusing on minimal nonequilibrium protocols that isolate intrinsic many-body dynamics. Quantum quenches, defined as sudden parameter changes, provide such a controlled framework [10–13]. By eliminating explicit driving fields, quenches directly expose fundamental nonequilibrium processes, including coherent many-body dynamics, relaxation pathways, dynamical criticality, and the emergence of nonthermal states. Among these, interaction quenches in the single-band Hubbard model [14] constitute a paradigmatic setting, as they probe the competition between kinetic energy and strong local correlations in its most direct form. These quenches are experimentally realizable in ultracold atomic systems via Feshbach tuning [15–18], establishing them as both conceptually clean and experimentally relevant probes of nonequilibrium correlated matter.

From the theoretical perspective, one-dimensional systems are relatively well understood [19–22]. In higher dimensions, however, controlled treatments of nonequilibrium dynamics remain challenging. Time-dependent dynamical mean-field theory (DMFT) has emerged as a cornerstone approach [23–29], capturing local quantum fluctuations exactly and revealing several robust features of interaction quenches, including nonequilibrium dynamical phase transitions, critical slowing down, and long-lived nonthermal states [30].

Despite these successes, DMFT and its cluster exten-

sions [28, 31] fundamentally either neglect or strongly constrain spatial fluctuations. As a result, they are intrinsically incapable of describing the spontaneous emergence of spatial inhomogeneities, such as domains, defects, or textured order, following a quench. This omission is not merely technical. General arguments [32–34] and experiments [35–37] indicate that quenches across or near instabilities naturally generate spatial structure. Moreover, a growing body of theoretical and numerical work demonstrates that quenched correlated systems—including superconducting, charge-ordered, and magnetically ordered phases—exhibit pronounced spatially inhomogeneous dynamics [38–44].

In the context of quench dynamics of Hubbard-type models, spatial inhomogeneities play a role in nonequilibrium dynamics that is conceptually analogous to that of quantum fluctuations: they provide essential relaxation channels and enable dephasing. At the same time, their inclusion allows for the emergence of nontrivial spatial textures that can qualitatively reshape post-quench evolution. Neglecting such effects can therefore lead to an incomplete, or even misleading, understanding of nonequilibrium behavior.

In this work, we address this gap by employing a real-space formulation of the time-dependent Gutzwiller approximation (TDGA) [45–47]. While TDGA neglects dynamical quantum fluctuations, it offers a substantial computational advantage that enables large-scale simulations with spatially resolved variational parameters. This makes it particularly well suited for studying nonequilibrium dynamics in the presence of spatial degrees of freedom, including the spontaneous development of inhomogeneities, spatial dephasing, and the emergence of long-lived textures following interaction quenches [48].

Within this framework, allowing spatial degrees of freedom qualitatively changes the long-time quench dynamics. While the early-time response remains coherent and consistent with homogeneous TDGA and DMFT benchmarks, the subsequent evolution is governed by spatial dephasing between locally oscillating regions, providing

an intrinsic relaxation channel even in the absence of dissipation [45]. In the intermediate-coupling regime, this leads to the nucleation and slow coarsening of Mott-like regions, producing long-lived inhomogeneous states that are inaccessible within spatially uniform approaches.

We consider the single-band Hubbard model on a triangular lattice,

$$H(t) = \sum_{\langle ij \rangle, \sigma} -t_{ij} c_{i\sigma}^\dagger c_{j\sigma} + U(t) \sum_i n_{i\uparrow} n_{i\downarrow}, \quad (1)$$

where $c_{i\sigma}^\dagger$ ($c_{i\sigma}$) creates (annihilates) an electron with spin σ at site i , t_{ij} denotes nearest-neighbor hopping (t_{nn}) and $U(t)$ is a time-dependent onsite interaction. Within the time-dependent Gutzwiller approximation (TDGA) [49–51], the many-body wavefunction is written as $|\Psi_G(t)\rangle = \hat{P}_G(t)|\Psi_S(t)\rangle$, where $|\Psi_S(t)\rangle$ is a Slater determinant and $\hat{P}_G(t)$ is a product of local Gutzwiller projectors parametrized by time-dependent variational amplitudes $\Phi_i(t)$, which play the role of slave-boson fields. The resulting effective description naturally separates into two coupled subsystems: quasiparticles evolving in the instantaneous background set by $\Phi_i(t)$, which renormalizes the hopping and on-site potentials of the effective quasiparticle Hamiltonian H_{qp} , and local Gutzwiller amplitudes $\Phi_i(t)$ that evolve under the feedback of the quasiparticle state through an effective slave-boson Hamiltonian H_{sb} . At any time, the quasiparticle density matrix $\rho_{j\sigma, i\sigma'} = \langle c_{i\sigma'}^\dagger c_{j\sigma} \rangle$ obeys a von Neumann equation,

$$\frac{d\rho}{dt} = i[\rho, H_{qp}(\{\Phi_i\})], \quad (2)$$

while the local Gutzwiller amplitudes evolve according to

$$\frac{d\Phi_i}{dt} = \frac{\partial}{\partial \Phi_i^\dagger} H_{sb}(\{\Phi_i\}, \rho). \quad (3)$$

These equations are solved simultaneously in real time, ensuring full self-consistency between quasiparticle motion and local correlation dynamics. We refer to this real-space implementation as the Gutzwiller von Neumann dynamics (GvND) method. Explicit expressions and numerical details are provided in the Appendix A.

We restrict ourselves to the paramagnetic regime. In this setting, the local Gutzwiller amplitudes can be taken in diagonal form, $\Phi_i(t) = \text{diag}(e_i, p_i, d_i)$, corresponding to empty, singly occupied, and doubly occupied local configurations, respectively. The system is initialized in the noninteracting ground state at zero temperature ($T = 0$) with interaction strength $U_i = 0$. At time $t = 0$, the interaction is suddenly quenched to a finite value U_f , and the system subsequently undergoes unitary time evolution governed by the interacting Hamiltonian.

To allow for the emergence of spatial dynamics without explicitly breaking symmetries, we introduce a weak on-site Anderson disorder potential ϵ_i with magnitude $10^{-5}t_{nn}$. All simulations are performed within the paramagnetic GvND framework on a 48×48 lattice. Time

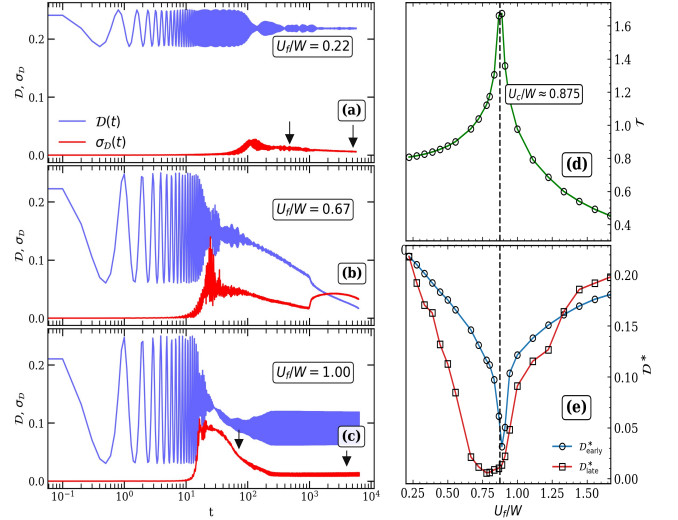


FIG. 1. GvND dynamics following an interaction quench to final strength U_f . Panels (a)–(c) show the time evolution of the double occupancy $\mathcal{D}(t)$ and its spatial standard deviation $\sigma_{\mathcal{D}}(t)$ for weak, intermediate, and strong quenches. Panel (d) shows the oscillation period \mathcal{T} extracted from the early-time dynamics as a function of U_f/W . Panel (e) shows the early-time and long-time averaged double occupancy D^* with varying U_f .

is measured in units of \hbar/t_{nn} throughout. We monitor the local density $n_i = |p_i|^2 + |d_i|^2$ and the local double occupancy $\mathcal{D}_i(t) = |d_i(t)|^2$. Details regarding timestep stability and numerical convergence are provided in the Appendix B.

We characterize the quench dynamics through the spatially averaged double occupancy $\mathcal{D}(t)$, shown in Fig. 1(a–c) for representative weak-, intermediate-, and strong-coupling interaction quenches. For all final interaction strengths, the evolution of $\mathcal{D}(t)$ exhibits a clear two-stage structure: an initial regime of coherent collective dynamics, followed at longer times by a qualitatively distinct regime dominated by spatial dephasing.

In the early-time regime, $\mathcal{D}(t)$ displays coherent oscillations characterized by a quench-dependent period \mathcal{T} and a reduced mean value D^* . This early-time behavior coincides with that obtained within homogeneous TDGA [45], reflecting a collective quasiparticle mode of the correlated state. The oscillation period displays a pronounced maximum as a function of the final interaction strength U_f [Fig. 1(d)], while the early-time averaged value D^* varies nonmonotonically with U_f [Fig. 1(e)], consistent with proximity to a dynamical critical point U_c . This provides our reference scale for classifying quenches as weak ($U \ll U_c$), intermediate ($U \approx U_c$), and strong ($U \gg U_c$). The redistribution of spectral weight and the associated renormalization of the effective bandwidth are discussed in the Appendix C.

We note that the inclusion of local quantum fluctuations can lead to damping of these early-time oscillations.

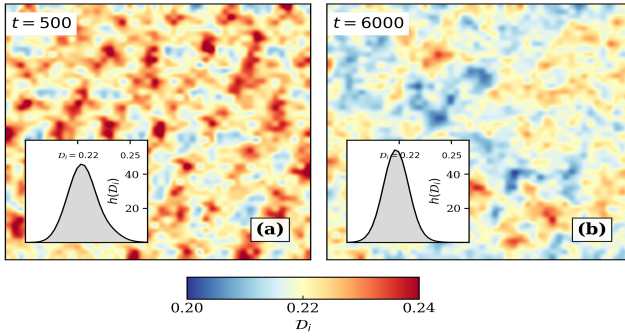


FIG. 2. Snapshots of the spatial distribution of the double occupancy $D(x,y)$ at intermediate time $t = 500$ and long time $t = 6000$ for interaction strength $U_f/W = 0.22$. The corresponding distributions of D are shown in the insets.

tions, as demonstrated in nonequilibrium DMFT simulations [30]. Such fluctuation-induced decoherence is expected to act as a seed for the subsequent emergence of spatial inhomogeneities, which we analyze below with the GvND framework.

At longer times, the post-quench dynamics enters a regime that departs qualitatively from the homogeneous description. The global oscillations of $D(t)$ collapse beyond a characteristic timescale, accompanied by a rapid growth of the spatial standard deviation $\sigma_D(t)$. This crossover marks the onset of spatial phase decoherence and the spontaneous development of inhomogeneity. Unlike in DMFT, the damping observed here originates from dephasing between locally oscillating regions rather than from local quantum dissipation. A detailed discussion of the interaction dependence of the early- and long-time regimes is provided in the Appendix D.

To elucidate the nature of the emergent inhomogeneity, we examine snapshots of the local double occupancy $D(x,y)$ at the times indicated by arrows in Fig. 1 for weak and strong quenches. Fig. 2 shows snapshots at intermediate and long times following a representative weak quench. At intermediate times, the system exhibits weak spatial modulations with approximately repeating patterns and small amplitude [Fig. 2(a)]. The corresponding distribution of D roughly assumes a Gaussian form. At long times, these modulations are washed out and no clear spatial correlations remain. The system evolves toward an approximately homogeneous quasi-stationary state, and the distribution of D becomes a slightly narrower Gaussian [Fig. 2(b)], consistent with spatial dephasing and the randomization of local phases.

For stronger quenches, the spatial dynamics changes qualitatively. The spatially averaged double occupancy $D(t)$ initially exhibits coherent oscillations, followed by a loss of global coherence as the spatial fluctuation $\sigma_D(t)$ grows, and eventually a partial recovery of coherence at long times as $\sigma_D(t)$ decreases. We focus on two representative stages of this evolution: an intermediate time after the loss of coherence and the long-time regime. As

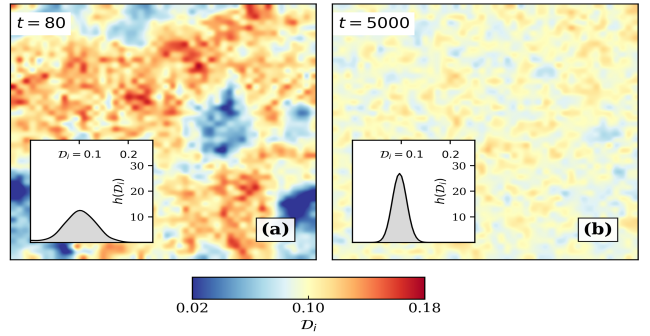


FIG. 3. Snapshots of the spatial distribution of the double occupancy $D(x,y)$ at intermediate time $t = 80$ and long time $t = 5000$ for interaction strength $U_f/W = 1.0$. The corresponding distributions of D are shown in the insets.

shown in Fig. 3(a), at intermediate times the system develops extended regions with strongly suppressed double occupancy coexisting with more itinerant regions, resulting in broad and distinctly non-Gaussian distributions of D_i . These inhomogeneities arise dynamically from unitary time evolution and are not induced by any externally imposed symmetry-breaking field. At long times, the spatial inhomogeneities are substantially reduced and the double occupancy recovers a finite value with a narrow, approximately Gaussian distribution [Fig. 3(b)]. Although this long-time state exhibits qualitative similarities to the early-time coherent regime, its properties are strongly renormalized by the transient inhomogeneous dynamics encountered at intermediate times.

The most pronounced deviations from homogeneous dynamics occur in the intermediate-coupling regime, where spatial inhomogeneities play a decisive role. While the qualitative growth and decay of $\sigma_D(t)$ are common to all interaction strengths, only in the intermediate regime do these fluctuations lead to nontrivial long-time dynamics. As shown in Fig. 4(a), the decay of the spatially averaged double occupancy around $t \simeq 800$ coincides with a sharp increase in $\sigma_D(t)$, signaling the onset of nucleation. In contrast, the charge density fluctuation $\sigma_n(t)$ decreases monotonically, indicating that the emerging structures are driven by correlation effects rather than charge redistribution. Snapshots of the local double occupancy D_i , shown in Fig. 4(b–e) and taken at the times marked by arrows in Fig. 4(a), reveal the formation of Mott-like regions that grow and merge over long timescales. Correspondingly, the probability distributions evolve from a broad single peak to a bimodal form dominated by a growing peak near $D \approx 0$, providing clear evidence for phase coexistence and slow coarsening.

Further support for this interpretation is provided by the probability distributions of the local double occupancy $D_i(t)$, shown in Fig. 5 for intermediate time windows. In the weak-coupling regime, the distribution is broader than a Gaussian, reflecting finite spatial fluctuations. In contrast, for strong quenches the instant-

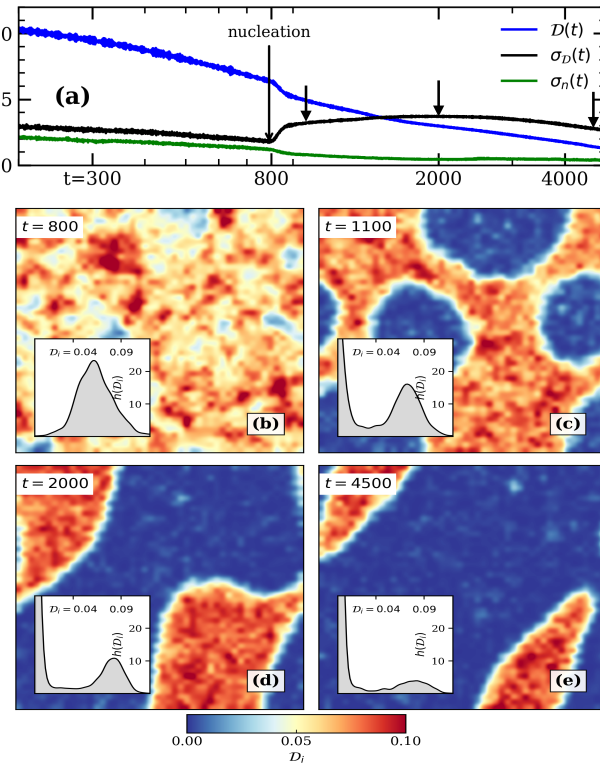


FIG. 4. Coarsening dynamics following a quench to $U_f/W = 0.72$. (a) Time evolution of the spatially averaged double occupancy $D(t)$, its spatial standard deviation $\sigma_D(t)$, and the density fluctuation $\sigma_n(t)$. (b)–(e) Snapshots of the local double occupancy D_i at the indicated times, showing domain nucleation followed by coarsening. Insets show the corresponding distributions of D_i .

taneous distributions remain narrow and approximately Gaussian; however, temporal oscillations of their mean lead to an effectively broadened, overlapping distribution upon time averaging. By comparison, the intermediate-coupling regime exhibits a distinctly bimodal structure, providing clear statistical evidence for the coexistence of Mott-like and itinerant regions during the post-quench evolution.

Taken together, Figs. 4 and 5 demonstrate that near the dynamical instability spatial inhomogeneities play a central role in shaping the long-time dynamics. The evolution proceeds via nucleation and coarsening rather than smooth relaxation, highlighting an intrinsic nonequilibrium instability of homogeneous solutions once spatial degrees of freedom are included, even in the absence of explicit dissipation.

The dynamical regimes identified here are separated by crossovers rather than sharp phase transitions, characterized by interaction-dependent timescales associated with the loss of global coherence and the growth of spatial inhomogeneities. While full thermalization is not expected within the GA framework, inclusion of spatial fluctuations opens additional relaxation channels through spa-

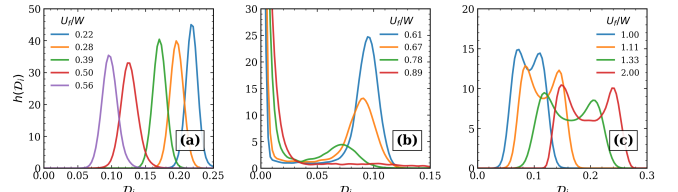


FIG. 5. Probability distributions of the local double occupancy $D_i(t)$ constructed from all sites of a 48×48 lattice and averaged over the time window $t \in [1000, 1100]$. Panels (a)–(c) correspond to quenches in the weak-, intermediate-, and strong-coupling regimes, respectively.

tial dephasing and redistribution of correlations. This suggests a route toward effective equilibration that is absent in spatially uniform treatments. The associated timescales may exhibit system-size dependence, as commonly observed in coarsening dynamics; a systematic analysis of finite-size effects is presented in the Appendix E, but a detailed scaling study is beyond the scope of the present work.

In summary, we have employed a real-space Gutzwiller–von Neumann dynamics approach to study interaction quenches in the half-filled Hubbard model on a triangular lattice. We find that the synchronized oscillatory dynamics predicted by spatially homogeneous theories is intrinsically unstable: even weak inhomogeneities are dynamically amplified, leading to spatial dephasing and the emergence of textured nonequilibrium states. Depending on the interaction strength, the post-quench evolution separates into three distinct dynamical regimes: weak quenches lead to nearly homogeneous relaxation, intermediate quenches exhibit nucleation and slow coarsening of Mott-like regions, and strong quenches display a collapse followed by a partial re-emergence of global coherence.

Our results highlight a complementary perspective to nonequilibrium DMFT. While DMFT emphasizes the role of local quantum fluctuations encoded along the imaginary-time axis, we demonstrate that purely real-space fluctuations can produce qualitatively similar relaxation phenomena through spatial dephasing and self-organization. An important open direction is to develop approaches that incorporate both spatial and quantum fluctuations on equal footing. More generally, our findings show that spatial self-organization is a key ingredient of far-from-equilibrium dynamics in correlated systems and must be explicitly accounted for in theoretical descriptions of driven quantum matter.

ACKNOWLEDGMENTS

This work was supported by the Owens Family Foundation. The authors acknowledge Research Computing at the University of Virginia for providing computational resources and technical support.

Appendix A: Real-Space Gutzwiller–von Neumann Dynamics Formalism

In this section we provide a detailed description of the real-space Gutzwiller–von Neumann dynamics (GvND) formalism employed in the main text. We consider the single-band Hubbard model

$$\hat{H}(t) = \sum_{ij,\sigma} -t_{ij} \hat{c}_{i\sigma}^\dagger \hat{c}_{j\sigma} + U(t) \sum_i \hat{n}_{i\uparrow} \hat{n}_{i\downarrow}, \quad (\text{A1})$$

where t_{ij} denotes the hopping amplitude between sites i and j , $U(t)$ is the (possibly time-dependent) onsite interaction, and $\hat{n}_{i\sigma} = \hat{c}_{i\sigma}^\dagger \hat{c}_{i\sigma}$.

The time-dependent Gutzwiller wave function is written as

$$|\Psi_G(t)\rangle = \hat{P}_G(t) |\Psi_S(t)\rangle, \quad (\text{A2})$$

where $|\Psi_S(t)\rangle$ is a Slater determinant describing itinerant quasiparticles and $\hat{P}_G(t) = \prod_i \hat{P}_i(t)$ is a product of local Gutzwiller projectors encoding correlation effects. Each local projector \hat{P}_i acts in the local Hilbert space $\{|0\rangle, |\uparrow\rangle, |\downarrow\rangle, |\uparrow\downarrow\rangle\}$ and is parametrized by a site-dependent variational matrix Φ_i .

This formulation is formally equivalent to the rotationally invariant slave-boson representation of correlated electron systems [48, 50]. Within this representation, expectation values of local operators reduce to traces over the local Hilbert space,

$$\langle \Psi_G | \hat{O}_i | \Psi_G \rangle = \text{Tr}(\hat{O}_i \Phi_i^\dagger \Phi_i). \quad (\text{A3})$$

Throughout this work we restrict to diagonal local correlators,

$$\hat{P}_i = \sum_{\Gamma} \Phi_{i\Gamma} |\Gamma\rangle_i \langle \Gamma|, \quad (\text{A4})$$

where Γ labels the four local charge configurations and the complex amplitudes $\Phi_{i\Gamma}$ control their statistical weights.

The equations of motion follow from the Dirac–Frenkel time-dependent variational principle [49, 52], applied to the action

$$\mathcal{S} = \int dt \langle \Psi_G(t) | i\partial_t - \hat{H}(t) | \Psi_G(t) \rangle. \quad (\text{A5})$$

Independent variation with respect to $|\Psi_S\rangle$ and Φ_i yields a closed set of coupled dynamical equations [45, 48]:

$$i\partial_t |\Psi_S\rangle = \hat{H}_{\text{GA}}[\{\Phi_i\}] |\Psi_S\rangle, \quad (\text{A6})$$

$$i\partial_t \Phi_i = \frac{\partial}{\partial \Phi_i^\dagger} \langle \hat{H}_{\text{GA}} \rangle, \quad (\text{A7})$$

where \hat{H}_{GA} is the effective Gutzwiller Hamiltonian.

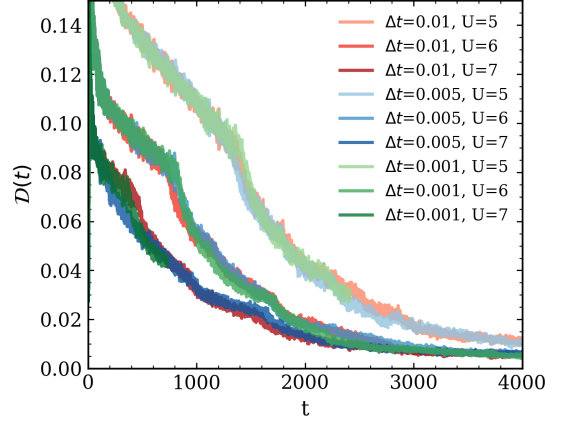


FIG. 6. Time evolution of the double occupancy $D(t)$ obtained using different timesteps $\Delta t = 0.001, 0.005$, and 0.01 for several U values, demonstrating numerical stability.

Within the Gutzwiller approximation, the latter takes the form

$$\hat{H}_{\text{GA}} = \sum_{ij,\sigma} -t_{ij} R_{i\sigma} R_{j\sigma}^* \hat{c}_{i\sigma}^\dagger \hat{c}_{j\sigma} + \sum_i U \hat{D}_i + \sum_{i\sigma} \mu_{i\sigma} \hat{n}_{i\sigma}, \quad (\text{A8})$$

where $\hat{D}_i = \text{diag}(0, 0, 0, 1)$ is the local double-occupancy operator and $\mu_{i\sigma}$ are Lagrange multipliers enforcing local charge constraints.

The hopping renormalization matrices $R_{i\sigma}$ encode the feedback of local correlations on quasiparticle motion and are defined as

$$R_{i,\alpha\beta} = \frac{\text{Tr}(\Phi_i^\dagger \hat{c}_{i\alpha}^\dagger \Phi_i \hat{c}_{i\beta})}{\sqrt{n_{i\beta}(1 - n_{i\beta})}}, \quad (\text{A9})$$

which for the single-band Hubbard model reduces to

$$R_{i,\sigma} = \frac{\Phi_{i0}^* \Phi_{i\sigma} + \Phi_{i\bar{\sigma}}^* \Phi_{i\uparrow\downarrow}}{\sqrt{n_{i\sigma}(1 - n_{i\sigma})}}. \quad (\text{A10})$$

We introduce the single-particle density matrix

$$\rho_{j\sigma,i\sigma'} = \langle \Psi_S | \hat{c}_{i\sigma'}^\dagger \hat{c}_{j\sigma} | \Psi_S \rangle, \quad (\text{A11})$$

whose time evolution obeys a von Neumann equation,

$$\frac{d\rho}{dt} = i[\rho, H_{\text{qp}}], \quad (\text{A12})$$

where,

$$[H_{\text{qp}}]_{i\sigma,j\sigma'} = -t_{i\sigma,j\sigma'} R_{i\sigma} R_{j\sigma'}^* + \mu_{i\sigma} \delta_{ij} \delta_{\sigma,\sigma'} \quad (\text{A13})$$

which constitutes the quasiparticle sector of the GvND dynamics [53]. Explicitly,

$$\begin{aligned} \frac{d\rho_{i\sigma,j\sigma}}{dt} = & i(\mu_{j\sigma} - \mu_{i\sigma}) \rho_{i\sigma,j\sigma} \\ & - i \sum_k (t_{ik} R_{i\sigma} R_{k\sigma}^* \rho_{k\sigma,j\sigma} - t_{kj} R_{k\sigma} R_{j\sigma}^* \rho_{i\sigma,k\sigma}). \end{aligned} \quad (\text{A14})$$

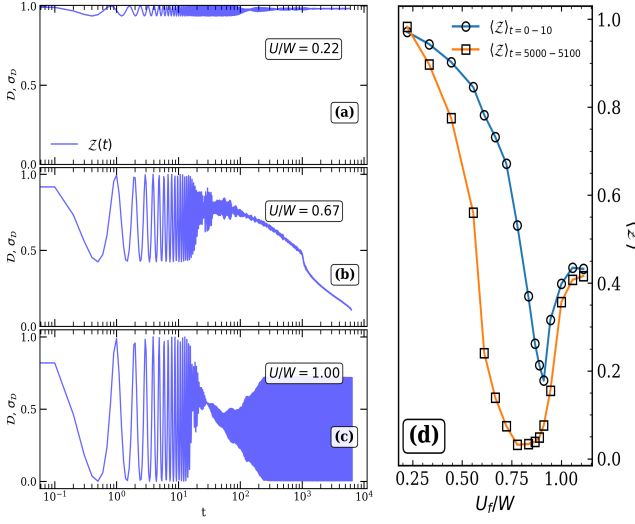


FIG. 7. Dynamics of the site-averaged spectral weight $Z(t)$ following an interaction quench to final strength U_f . Panels (a)–(c) show $Z(t)$ for weak, intermediate, and strong quenches, respectively. Panel (d) shows the early-time and long-time averaged spectral weight $\langle Z \rangle$ as a function of U_f/W .

Using Eq. (A8), the equation of motion for the local Gutzwiller amplitudes becomes

$$\begin{aligned} i \frac{d\Phi_i}{dt} &= U \hat{D} \Phi_i - \sum_{j\sigma} t_{ij} \frac{\partial R_{i\sigma}}{\partial \Phi_i^\dagger} R_{j\sigma}^* \rho_{ji} - \sum_{\sigma} \mu_{i\sigma} \hat{N}_{\sigma} \Phi_i \\ &= \frac{\partial}{\partial \Phi_i^\dagger} H_{\text{sb}}, \end{aligned} \quad (\text{A15})$$

which closes the coupled dynamics of quasiparticles and local correlation fields.

In this work we restrict to paramagnetic states, imposing

$$\begin{aligned} n_{i\uparrow} &= n_{i\downarrow} \equiv n_i, \\ \Phi_{i0} &= e_i, \quad \Phi_{i\uparrow} = \Phi_{i\downarrow} = p_i, \quad \Phi_{i\uparrow\downarrow} = d_i. \end{aligned} \quad (\text{A16})$$

leading to

$$R_i = \frac{e_i^* p_i + p_i^* d_i}{\sqrt{n_i(1-n_i)}}. \quad (\text{A17})$$

The TDGA equations possess a local gauge freedom associated with the phase of Φ_i . For paramagnetic states the chemical potentials satisfy

$$\mu_{i\uparrow} = \mu_{i\downarrow} \equiv \mu_i, \quad (\text{A18})$$

with the explicit expression [54]

$$\mu_i = \frac{n_i - \frac{1}{2}}{n_i(1-n_i)} \text{Re}(\Lambda_i R_i), \quad (\text{A19})$$

where

$$\Lambda_i = \sum_j -t_{ij} R_j^* \rho_{ij}. \quad (\text{A20})$$

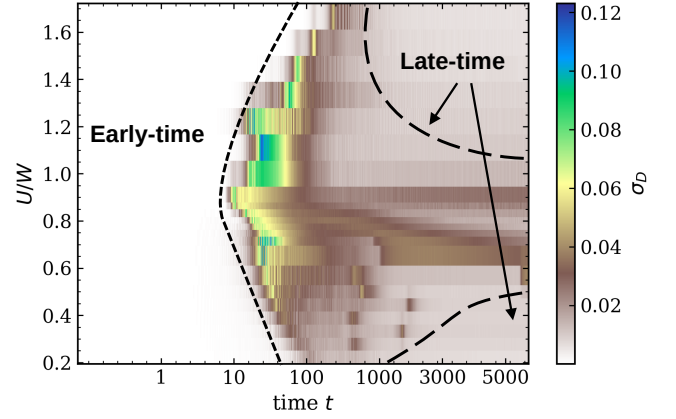


FIG. 8. Color map of the spatial fluctuation of double occupancy, $\sigma_D(t)$, as a function of time t and interaction strength U_f/W . Dashed lines indicate the approximate boundaries separating the early- and late-time homogeneous regimes from the intermediate-time inhomogeneous regime.

Appendix B: Numerical implementation

In numerical simulations, Eqs. (A14) and (A15) are integrated simultaneously in time, ensuring full self-consistency between quasiparticle motion and local correlation dynamics. This real-space implementation constitutes the Gutzwiller–von Neumann dynamics method used throughout the main text.

The Hamiltonian contains two independent energy scales: the nearest-neighbor hopping t_{nn} and the onsite interaction U . We set $t_{nn} = 1$, thereby measuring time in units of \hbar/t_{nn} , and normalize the interaction strength by the uncorrelated bandwidth $W = 9t_{nn}$ appropriate for the triangular lattice. All results are therefore reported in terms of U/W and dimensionless time t , unless mentioned otherwise.

The coupled equations of motion are solved using a fourth-order Runge–Kutta scheme with timestep Δt . To verify numerical stability and convergence, we perform simulations for $\Delta t = 0.001, 0.005$, and 0.01 on a small system of size 12×12 . As shown in Fig. 6, these choices yield quantitatively similar trajectories for the observables reported in the main text.

To seed spatial dynamics without explicitly breaking symmetries, we introduce a weak on-site Anderson disorder potential $\{\epsilon_i\}$, whose magnitude is varied across simulations while keeping $\epsilon/W \sim 10^{-6}$. The results reported are insensitive to the specific realization or precise amplitude of this weak disorder.

Appendix C: Spectral Weight

Within the Gutzwiller approximation, correlation effects renormalize the hopping amplitudes according to $t_{ij} \rightarrow t_{ij} R_i R_j^*$, where the site-dependent factors R_i en-

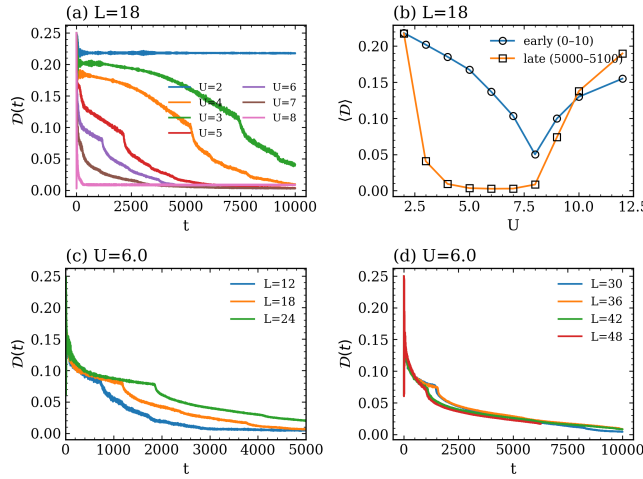


FIG. 9. System-size dependence of the double occupancy dynamics. (a) $\mathcal{D}(t)$ for an 18×18 lattice at different interaction strengths. (b) Early-time ($t \in [0, 10]$) and late-time ($t \in [5000, 5100]$) averages of \mathcal{D} versus U_f . (c),(d) Size dependence of $\mathcal{D}(t)$ near intermediate coupling, showing faster relaxation for smaller systems and weak size dependence for $L \gtrsim 30$.

code the reduction of quasiparticle coherence due to local correlations. A useful global measure of this renormalization is the site-averaged spectral weight, $\mathcal{Z}(t) = |\langle R_i(t) \rangle|^2$, which directly reflects the effective bandwidth of the correlated quasiparticles.

Figure 7 shows the time evolution of $\mathcal{Z}(t)$ following interaction quenches of varying strength. At early times, $\mathcal{Z}(t)$ exhibits coherent oscillations that closely follow the predictions of homogeneous TDGA, consistent with the behavior of the double occupancy discussed in the main text. At longer times, however, $\mathcal{Z}(t)$ departs from the homogeneous TDGA dynamics, reflecting the growth of spatial inhomogeneities and the breakdown of synchronized quasiparticle motion.

Panel 7(d) summarizes the early- and long-time averaged spectral weight as a function of U_f/W . The pronounced deviation between the two regimes mirrors the behavior observed for the double occupancy, further confirming that spatial dephasing and inhomogeneity lead to an effective renormalization of quasiparticle coherence beyond homogeneous descriptions.

Appendix D: Temporal regimes

Figure 8 shows the time evolution of the spatial fluctuation of double occupancy, $\sigma_{\mathcal{D}}(t)$, as a color map for varying interaction strength U_f/W . This representation highlights the separation between distinct temporal regimes in the post-quench dynamics. At early times, $\sigma_{\mathcal{D}}(t)$ remains vanishingly small for all interaction strengths, indicating nearly homogeneous dynamics consistent with the predictions of spatially uniform TDGA. The extent of this early-time regime is strongly interaction dependent, as indicated by the dashed boundary.

At longer times, spatial inhomogeneities develop in an interaction-dependent manner. For weak and strong quenches, $\sigma_{\mathcal{D}}(t)$ approaches a small but finite value that remains approximately time independent at late times, as marked by the long dashed guide lines. In contrast, for intermediate interaction strengths, $\sigma_{\mathcal{D}}(t)$ continues to evolve over the entire simulation window and does not reach an apparent asymptotic value. This persistent growth reflects the slow nucleation and coarsening dynamics discussed in the main text.

Appendix E: System-size effects

Figure 9 illustrates the dependence of the post-quench dynamics on system size. Panel (a) shows the time evolution of the spatially averaged double occupancy $\mathcal{D}(t)$ for an 18×18 lattice over long times ($t \leq 10^4$) and for several interaction strengths. While the initial decay and early-time behavior are similar across different U_f , the long-time evolution exhibits a pronounced dependence on interaction strength.

This behavior is summarized in Fig. 9(b), which compares the early-time and late-time averages of \mathcal{D} as a function of U_f . The late-time values show a markedly different dependence on U_f , particularly in the intermediate-coupling regime where \mathcal{D} remains strongly suppressed.

Panels (c) and (d) show the size dependence of $\mathcal{D}(t)$ near intermediate coupling for different linear system sizes L . For smaller systems, the decay of $\mathcal{D}(t)$ occurs more rapidly, while increasing the system size leads to a slower evolution at long times. For $L \gtrsim 30$, the time dependence of $\mathcal{D}(t)$ becomes comparatively weak within the accessible simulation time window, indicating reduced finite-size effects in this regime.

[1] J. Eisert, M. Friesdorf, and C. Gogolin, Quantum many-body systems out of equilibrium, *Nature Physics* **11**, 124 (2015).
[2] D. N. Basov, R. D. Averitt, D. van der Marel, M. Dresel, and K. Haule, Electrodynamics of correlated electron materials, *Rev. Mod. Phys.* **83**, 471 (2011).
[3] A. Polkovnikov, K. Sengupta, A. Silva, and M. Ven- galattore, Nonequilibrium dynamics of closed interacting quantum systems, *Reviews of Modern Physics* **83**, 863 (2011).
[4] J. Bloch, A. Cavalleri, V. Galitski, M. Hafezi, and A. Rubio, Strongly correlated electron–photon systems, *Nature* **606**, 41–48 (2022).
[5] F. Boschini, M. Zonno, and A. Damascelli, Time-resolved

arpes studies of quantum materials, *Rev. Mod. Phys.* **96**, 015003 (2024).

[6] S. Buschhorn, F. Brüssing, R. Abrudan, and H. Zabel, Adaption of a diffractometer for time-resolved X-ray resonant magnetic scattering, *Journal of Synchrotron Radiation* **18**, 212 (2011).

[7] J. Orenstein and J. S. Dodge, Terahertz time-domain spectroscopy of transient metallic and superconducting states, *Phys. Rev. B* **92**, 134507 (2015).

[8] I. P. Parkin, Q. A. Pankhurst, L. Affleck, M. D. Aguas, and M. V. Kuznetsov, Self-propagating high temperature synthesis of bafeo, mgznfeo and lifeo; time resolved x-ray diffraction studies (trxd), *J. Mater. Chem.* **11**, 193 (2001).

[9] A. Vernes and P. Weinberger, Formally linear response theory of pump-probe experiments, *Phys. Rev. B* **71**, 165108 (2005).

[10] A. Mitra, Quantum quench dynamics, *Annual Review of Condensed Matter Physics* **9**, 245 (2018).

[11] T. Mori, T. N. Ikeda, E. Kaminishi, and M. Ueda, Thermalization and prethermalization in isolated quantum systems: a theoretical overview, *Journal of Physics B: Atomic, Molecular and Optical Physics* **51**, 112001 (2018).

[12] C. Gogolin and J. Eisert, Equilibration, thermalisation, and the emergence of statistical mechanics in closed quantum systems, *Reports on Progress in Physics* **79**, 056001 (2016).

[13] R. Vasseur and J. E. Moore, Nonequilibrium quantum dynamics and transport: from integrability to many-body localization, *Journal of Statistical Mechanics: Theory and Experiment* , 064010 (2016).

[14] J. Hubbard, Electron correlations in narrow energy bands, *Proceedings of the Royal Society of London. Series A. Mathematical and Physical Sciences* **276**, 238 (1963).

[15] T. Langen, R. Geiger, and J. Schmiedmayer, Ultracold atoms out of equilibrium, *Annual Review of Condensed Matter Physics* **6**, 201 (2015).

[16] I. Bloch, J. Dalibard, and W. Zwerger, Many-body physics with ultracold gases, *Reviews of Modern Physics* **80**, 885 (2008).

[17] T. Esslinger, Fermi-hubbard physics with ultracold atoms in optical lattices, *Annual Review of Condensed Matter Physics* **1**, 129 (2010).

[18] M. Greiner, O. Mandel, T. Esslinger, T. W. Hänsch, and I. Bloch, Collapse and revival of the matter wave field of a bose-einstein condensate, *Nature* **419**, 51 (2002).

[19] A. Takahashi, H. Itoh, and M. Aihara, Photoinduced insulator-metal transition in one-dimensional mott insulators, *Physical Review B* **77**, 205105 (2008).

[20] S. Ejima, F. Lange, and H. Fehske, Photoinduced metallization of excitonic insulators, *Physical Review B* **105**, 245126 (2022).

[21] S. R. White and A. E. Feiguin, Real-time evolution using the density matrix renormalization group, *Physical Review Letters* **93**, 076401 (2004).

[22] A. J. Daley, C. Kollath, U. Schollwöck, and G. Vidal, Time-dependent density-matrix renormalization-group using adaptive effective hilbert spaces, *Journal of Statistical Mechanics: Theory and Experiment* , P04005 (2004).

[23] H. Aoki, N. Tsuji, M. Eckstein, M. Kollar, T. Oka, and P. Werner, Nonequilibrium dynamical mean-field theory and its applications, *Reviews of Modern Physics* **86**, 779 (2014).

[24] D. Afanasiev, A. Gatilova, et al., Ultrafast spin dynamics in photodoped spin-orbit mott insulator sr_2iro_4 , *Physical Review X* **9**, 021020 (2019).

[25] P. Werner, N. Tsuji, and M. Eckstein, Nonthermal symmetry-broken states in the strongly interacting hubbard model, *Physical Review B* **86**, 205101 (2012).

[26] J. H. Mentink and M. Eckstein, Ultrafast quenching of the exchange interaction in a mott insulator, *Physical Review Letters* **113**, 057201 (2014).

[27] K. Balzer, F. A. Wolf, I. P. McCulloch, P. Werner, and M. Eckstein, Nonthermal melting of néel order in the hubbard model, *Physical Review X* **5**, 031039 (2015).

[28] M. Eckstein and P. Werner, Ultrafast photo-carrier relaxation in mott insulators with short-range spin correlations, *Scientific Reports* **6**, 21235 (2016).

[29] J. K. Freericks, V. M. Turkowski, and V. Zlatić, Nonequilibrium dynamical mean-field theory, *Physical Review Letters* **97**, 266408 (2006).

[30] M. Eckstein, M. Kollar, and P. Werner, Thermalization after an interaction quench in the hubbard model, *Phys. Rev. Lett.* **103**, 056403 (2009).

[31] A. I. Lichtenstein and M. I. Katsnelson, Antiferromagnetism and d-wave superconductivity in cuprates: Cluster dynamical mean-field theory, *Physical Review B* **62**, R9283 (2000).

[32] W. H. Zurek, U. Dorner, and P. Zoller, Dynamics of a quantum phase transition, *Physical Review Letters* **95**, 105701 (2005).

[33] W. H. Zurek, Cosmological experiments in superfluid helium?, *Nature* **317**, 505 (1985).

[34] J. Dziarmaga, Dynamics of a quantum phase transition and relaxation to a steady state, *Advances in Physics* **59**, 1063 (2010).

[35] C. N. Weiler, T. W. Neely, D. R. Scherer, A. S. Bradley, M. J. Davis, and B. P. Anderson, Spontaneous vortices in the formation of bose-einstein condensates, *Nature* **455**, 948 (2008).

[36] G. Lamporesi, S. Donadello, S. Serafini, F. Dalfovo, and G. Ferrari, Spontaneous creation of kibble-zurek solitons in a bose-einstein condensate, *Nature Physics* **9**, 656 (2013).

[37] I. Chuang, R. Durrer, N. Turok, and B. Yurke, Cosmology in the laboratory: Defect dynamics in liquid crystals, *Science* **251**, 1336 (1991).

[38] G.-W. Chern and K. Barros, Nonequilibrium dynamics of superconductivity in the attractive hubbard model, *Physical Review B* **99**, 035162 (2019).

[39] B. Huang, X. Yang, N. Xu, J. Zhou, and M. Gong, Dynamical instability with respect to finite-momentum pairing in quenched bcs superconducting phases, *Physical Review B* **99**, 014517 (2019).

[40] L. Yang and G.-W. Chern, Photoinduced pattern formation and melting of charge density wave order, *Physical Review B* **111**, 094208 (2025).

[41] B. Fan and A. M. G. García, Quenched dynamics and pattern formation in clean and disordered bogoliubov-de gennes superconductors, *SciPost Physics* **17**, 049 (2024).

[42] L. Yang, Y. Yang, and G.-W. Chern, Pattern formation in charge density wave states after a quantum quench, *Physical Review B* **109**, 195133 (2024).

[43] S. S. Bakshi, T. Mondal, and P. Majumdar, Dynamics in the nonequilibrium energy landscape of a frustrated mott insulator, arXiv preprint (2024), arXiv:2409.05555

[cond-mat.str-el].

[44] S. S. Bakshi and P. Majumdar, Distinct charge and spin recovery dynamics in a photoexcited mott insulator, *Physical Review Letters* **133**, 256501 (2024).

[45] M. Schiró and M. Fabrizio, Time-dependent mean-field theory for quench dynamics in correlated electron systems, *Physical Review Letters* **105**, 076401 (2010).

[46] M. Schiró and M. Fabrizio, Quantum quenches in the hubbard model: Time-dependent mean-field theory and the role of quantum fluctuations, *Physical Review B* **83**, 165105 (2011).

[47] M. Sandri and M. Fabrizio, Nonequilibrium dynamics in the antiferromagnetic hubbard model, *Physical Review B* **88**, 165113 (2013).

[48] G. Seibold and J. Lorenzana, Time-dependent gutzwiller approximation for the hubbard model, *Physical Review Letters* **86**, 2605 (2001).

[49] J. Frenkel, Wave Mechanics: Advanced General Theory (Clarendon Press, Oxford, 1934).

[50] G. Kotliar and A. E. Ruckenstein, New functional integral approach to strongly correlated fermi systems: The gutzwiller approximation as a saddle point, *Physical Review Letters* **57**, 1362 (1986).

[51] T. Li, P. Wölfle, and P. J. Hirschfeld, Spin-rotation-invariant slave-boson approach to the hubbard model, *Physical Review B* **40**, 6817 (1989).

[52] P. A. M. Dirac, Note on exchange phenomena in the thomas atom, *Math. Proc. Cambridge Philos. Soc.* **26**, 376 (1930).

[53] G.-W. Chern, Dynamic inhomogeneities and phase separation after quantum quenches in strongly correlated systems, arXiv preprint (2017), arXiv:1711.07972 [cond-mat.str-el].

[54] N. Lanatà, Y. Yao, X. Deng, V. Dobrosavljević, and G. Kotliar, Slave boson theory of orbital differentiation with crystal field effects: Application to UO_2 , *Physical Review Letters* **118**, 126401 (2017).